

Polarization Patterns in Pulsar Radio Emission

Mark M. McKinnon

National Radio Astronomy Observatory,¹ Socorro, NM 87801 USA

ABSTRACT

A variety of intriguing polarization patterns are created when polarization observations of the single pulses from radio pulsars are displayed in a two-dimensional projection of the Poincaré sphere. In many pulsars, the projections produce two clusters of data points that reside at antipodal points on the sphere. The clusters are formed by fluctuations in polarization amplitude that are parallel to the unit vectors representing the polarization states of the wave propagation modes in the pulsar magnetosphere. In other pulsars, however, the patterns are more complex, resembling annuli and bow ties or bars. The formation of these complex patterns is not understood and largely unexplored. An empirical model of pulsar polarization is used to show that these patterns arise from polarization fluctuations that are perpendicular to the mode vectors. The model also shows that the modulation index of the polarization amplitude is an indicator of polarization pattern complexity. A stochastic version of generalized Faraday rotation can cause the orientation of the polarization vectors to fluctuate and is a possible candidate for the perpendicular fluctuations incorporated in the model. Alternative models indicate that one mode experiences perpendicular fluctuations and the other does not, suggesting that the fluctuations could also be due to a mode-selective random process, such as scattering in the magnetosphere. A polarization stability analysis of the patterns implies that processes intrinsic to the emission are more effective in depolarizing the emission than fluctuations in the orientation of its polarization vector.

Subject headings: methods: analytical – polarization – plasmas – pulsars: general – pulsars:individual (PSR B0823+26, PSR B1929+10, PSR B2020+28)

¹The National Radio Astronomy Observatory is a facility of the National Science Foundation operated under cooperative agreement by Associated Universities, Inc.

1. INTRODUCTION

Pulsar radio emission is renowned for its complicated polarization behavior. The polarization is generally elliptical, yet predominantly linear, and highly variable, often switching between two, orthogonally polarized states (e.g. Stinebring et al. 1984). A recent trend in the display and interpretation of the results from polarization observations of individual pulses has been to plot the measured values of the polarization vector’s orientation angles at a given rotational phase of the pulse in a two-dimensional projection of the Poincaré sphere. The projections reveal a wide variety of organized polarization patterns. For example, towards the center of the pulse in PSR B2020+28, the angles reside in a single cluster in one hemisphere of the Poincaré sphere (McKinnon 2004). The orientation angles form a diffuse structure resembling a bow tie near the pulse center of PSR B0818–13 (Edwards 2004). At the peak of PSR B1133+16, a Hammer-Aitoff projection of the angles produces two data clusters, each in a separate hemisphere of the Poincaré sphere (Karastergiou et al. 2003). The Lambert equal-area projections (LEAPs) of the orientation angles in PSR B0329+54 reveal two extremes in polarization behavior within the pulsar’s pulse (Edwards & Stappers 2004). In the cone emission on the edges of the pulse, the angles reside in two, circularly-shaped, bipolar clusters, similar to the angles in PSR B1133+16. But within the pulsar’s core emission at the pulse center, one of the two clusters stretches into an ellipse or bar, while the other spreads into an intriguing partial annulus. An accurate description of these patterns is needed to determine the physical processes that create them.

The origin of the simple polarization patterns is generally understood within the context of the statistical model of McKinnon & Stinebring (1998, 2000), aided by the analyses of McKinnon (2004) and Edwards & Stappers (2004). A single, compact cluster is produced when the fluctuations in the Stokes parameters Q , U , and V are comparable to one another, but less than the mean value of the polarization vector’s amplitude, as might be expected for the measurement of a polarization vector with fixed amplitude and orientation accompanied by instrumental noise. Orthogonal polarization modes (OPMs) produce the projections showing two clusters of orientation angles. The unit vectors representing the mode polarizations are antiparallel to each other and form a diagonal in the Poincaré sphere. Since the mode vectors are antiparallel, the amplitude of the resultant polarization is the difference between the mode polarization amplitudes, and the tip of the resultant polarization vector will reside in one hemisphere of the Poincaré sphere or the other depending upon which mode is the stronger of the two. The instantaneous orientation of the polarization vector alternates randomly between hemispheres due to temporal fluctuations in the polarized intensity of each mode that could be caused by the radio emission mechanism or propagation effects in the pulsar magnetosphere, such as the birefringence of the modes (e.g. Allen & Melrose 1982; Barnard & Arons 1986). The resulting polarization fluctuations caused by the

OPMs are therefore parallel to the mode diagonal.

The clues to the origin of the more complicated polarization patterns are provided in the analyses of McKinnon (2004) and Edwards & Stappers (2004), the polarization observations of Edwards (2004), and the numerical simulations of Melrose et al. (2006). The shape of the Q-U-V data point clusters created by the polarization fluctuations is generally an ellipsoid. McKinnon and Edwards & Stappers independently developed a technique to quantify the polarization fluctuations by measuring the ellipsoid’s dimensions. The technique calculates the covariance matrix of the Stokes parameters and subsequently determines the matrix eigenvalues. The three dimensions of the polarization ellipsoid are related to the eigenvalues, and the eigenvectors are the three orthogonal axes of the ellipsoid. For some objects, such as PSR B0809+74 (Edwards 2004), PSR B1929+10, and PSR B2020+28 (McKinnon 2004), two of the eigenvalues are roughly equal but less than the third, which is what one would expect for a prolate ellipsoid fashioned by OPMs. But Edwards (2004) also found examples (e.g. PSR B0320+39 and PSR B0818–13) where all three eigenvalues are different, proving that the polarization fluctuations possess a component that is *perpendicular* to the mode diagonal, in addition to the *parallel* component produced by the OPMs. Melrose et al. (2006) had to incorporate fluctuations in the orientation of the mode diagonal to replicate the polarization patterns observed by Edwards & Stappers in PSR B0329+54. Randomly varying orientation angles equate to both parallel and perpendicular components in the polarization fluctuations. Karastergiou et al. (2003) also suggested that random variations in the orientation of the mode diagonal might be needed to explain their observations of PSR B1133+16.

McKinnon & Stinebring (1998; 2000) proposed that the polarization of the radio emission is determined by the incoherent superposition of two, highly polarized, orthogonal modes. The assumption of highly polarized modes has strong theoretical support on the grounds that any plasma has two natural modes of wave propagation that are completely polarized (Petrova 2001). The assumption of incoherent modes means the modes propagate independently, which has two important consequences. First, when the radiation components are independent, the intensity of the combined radiation is the sum of the intensities of the individual radiation components (Chandrasekhar 1960; Ishimaru 1978). This realization simplifies the modeling of the radiation and its polarization. Second, the independence of the modes requires the difference in mode phases to be greater than unity. The mode phase difference, $\Delta\chi = \Delta kL$, is the product of the difference between the mode wave numbers, Δk , in the plasma and the distance, L , the modes propagate through the plasma. Generalized Faraday rotation (GFR) has been defined as the physical process responsible for creating the difference in mode phases (Melrose 1979). If this definition is correct, then GFR must be operative in the pulsar magnetosphere. Stochastic GFR can also alter the orientation of the polarization vector and, therefore, is a tantalizing prospect for the origin

of some polarization patterns we observe (Edwards & Stappers 2004).

Melrose et al. (2006) made great strides in simulating the polarization patterns with their numerical model and called for further use of empirical models to constrain the mechanism that leads to the separation of the modes. The objective of this paper is to incorporate the perpendicular fluctuations in an analytical model of pulsar polarization in an attempt to replicate the observed polarization patterns and identify potential processes responsible for the fluctuations. The perpendicular fluctuations are incorporated in the model in §2. The polarization patterns produced by different fluctuation geometries are also determined. The fluctuations can depolarize the emission, and, in §3, the depolarization is quantified with a polarization stability factor for most of the fluctuation geometries. In §4, the perpendicular fluctuations are interpreted in the context of stochastic GFR or scattering in the pulsar magnetosphere. The results and implications of the analysis are discussed in §5. Conclusions are summarized in §6. The Appendix lists the joint probability densities of the polarization vector’s orientation angles for each of the fluctuation geometries.

2. ANALYTICAL MODEL OF POLARIZATION PATTERNS

The polarization patterns are two-dimensional representations of the joint probability density of the polarization vector’s longitude, ϕ , and colatitude, θ . The functional form of the joint probability density can be estimated from a statistical model of pulsar polarization. An analytical, empirical model of pulsar polarization has been summarized in McKinnon (2003). Here, the model is generalized to accommodate polarization fluctuations perpendicular to the mode diagonal.

The Stokes parameters Q , U , and V completely describe the polarization of the radiation. The measured values of Q , U , and V are the linear sums of the pulsar-intrinsic polarization fluctuations and the instrumental noise. An analytical description of many types of polarization patterns can be determined by assuming that all fluctuations are independent, normal random variables (RVs). Since the sum of independent, normal RVs is also a normal RV, this assumption allows us to interpret the polarization as being composed of fixed and fluctuating parts, where the fluctuations follow a normal distribution. The fixed part is the mean value, μ , of the polarization vector amplitude. The analysis can be simplified by defining a new Cartesian coordinate system, q , u , and v , within the Poincaré sphere where the new v -axis is aligned with the mean orientation of the polarization vector. The simple equations that specify the model are then

$$q = x_q, \tag{1}$$

$$u = x_u, \tag{2}$$

$$\mathbf{v} = \mu + x_v. \quad (3)$$

The normal RVs x account for the polarization fluctuations in each of q , u , and v . They each have a zero mean, and their standard deviations are denoted by σ_q , σ_u , and σ_v in what follows. The q , u , v coordinate system forms the eigenbasis of the polarization ellipsoid, and σ_q , σ_u , and σ_v are the square roots of its eigenvalues (McKinnon 2004; Edwards & Stappers 2004). Equations 1-3 give the Cartesian coordinates that define the instantaneous orientation and amplitude of the polarization vector. The joint probability density of the vector’s orientation angles can be computed by a transformation from Cartesian to spherical coordinates.

Five cases with different fluctuation geometries, from simple to complex, are explored in the subsections that follow. Four cases investigate possible geometries where at least two of the eigenvalues are equal. The fifth case is more general, and evaluates a scenario where all the eigenvalues are different. Granted, other cases could be considered, but they generally produce patterns that are simple rotations of the patterns produced here. The cases show that the polarization pattern is determined by the relative magnitudes of σ_q , σ_u , and σ_v and the value of μ .

Despite the simplicity of Equations 1-3, the joint density produced from them has a complicated mathematical form. Interestingly, but quite understandably, the mathematical form of the joint density is basically the same in all cases, differing only in a parameterization determined by the geometry of the polarization fluctuations. The form of the joint density and its geometrical parameterization for all cases considered is given in the Appendix. The functional form of the joint density can be captured in a much simpler conditional density, which is the probability density of the orientation angles at a fixed value of the polarization amplitude, r_o . The detailed procedure for calculating both the joint and conditional densities is described in McKinnon (2003, 2006) and is not reproduced here. The conditional probability densities of the orientation angles are derived for each case below.

Table 1 summarizes the results obtained for each case by listing the resulting shape of the q - u - v ellipsoid and the formal name of the orientation angles’ conditional density. The axis orientation in the table describes the orientation of the ellipsoid’s axis of symmetry with respect to the v axis.

Figures 1 and 2 show LEAP examples for each case. A LEAP is simply a polar plot where a data point’s azimuth is ϕ and its radius is $2 \sin(\theta/2)$. The most attractive feature of a LEAP is it preserves the density of data points on the sphere when projecting them in two dimensions (Fisher et al. 1987). In the figures, the left side of the LEAP is the projection of the top hemisphere of the q - u - v sphere as viewed down the v axis, where $\theta = 0$. The right side of the LEAP is the projection of the bottom hemisphere at $\theta = \pi$. The circular edge of the projections is the equator of the q - u - v sphere, where $\theta = \pi/2$.

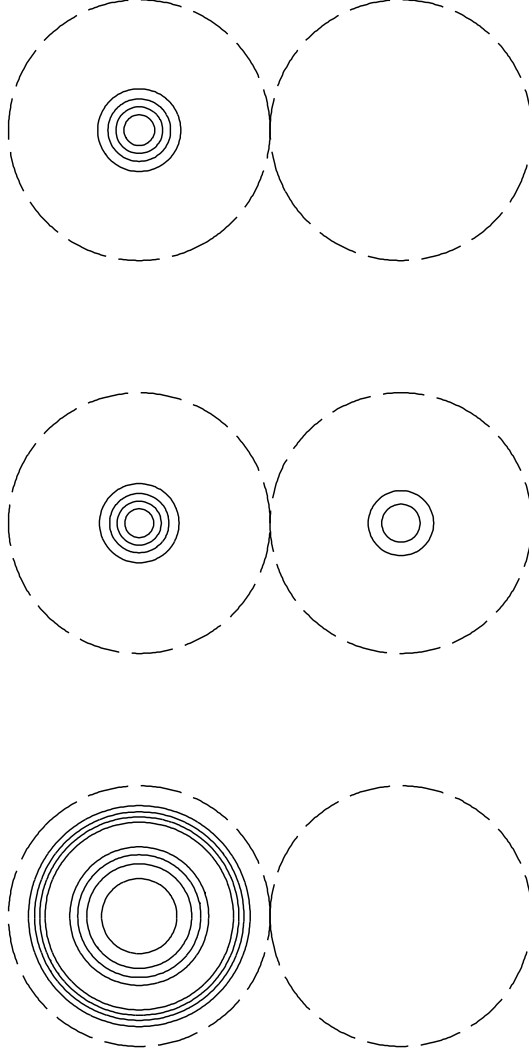


Fig. 1.— Examples of possible polarization patterns in pulsar radio emission. The patterns are shown as contour plots of Lambert equal area projections of the Poincaré sphere. *Top panel:* Fisher distribution with $\kappa = 4$ (Case 1). *Middle panel:* Bingham-Mardia bipolar distribution with $\kappa = 3, \gamma = 0.015$ created by fluctuations parallel to the polarization vector (Case 2). *Bottom panel:* Bingham-Mardia girdle distribution with $\kappa = 4, \gamma = 0.6$ created by fluctuations perpendicular to the polarization vector (Case 3). Contour levels are at 0.2, 0.4, 0.6, and 0.8 of the peak value in each projection.

2.1. Case 1: $\sigma_q = \sigma_u = \sigma_v$

The first case to consider is the simplest of the five, and evaluates the conditional density when the standard deviations of the polarization fluctuations are identical (i.e. $\sigma_q = \sigma_u = \sigma_v = \sigma$). The shape of the q-u-v cluster in this case is a spheroid because the standard deviations are equal. Since the cluster is a spheroid, it does not have a unique symmetry axis. This case was evaluated by McKinnon (2003), and represents the statistics of a fixed polarization vector accompanied by instrumental noise. The conditional density of the polarization vector’s orientation angles is a Fisher distribution

$$f_1(\theta, \phi | r_o) = \frac{\sin \theta}{4\pi} \frac{\kappa^2 \exp(\kappa^2 \cos \theta)}{\sinh(\kappa^2)}, \quad (4)$$

where

$$\kappa^2 = \frac{\mu r_o}{\sigma^2}. \quad (5)$$

The parameter κ^1 is inversely related to the conditional density’s standard deviation. Since $\sin \theta$ is proportional to the derivative of $\cos \theta$, the Fisher distribution is an exponential in $\cos \theta$. The density is not a function of ϕ because the distribution of data points is azimuthally symmetric about the mean orientation of the polarization vector (i.e. ϕ is uniformly distributed over 2π and is independent of θ). Therefore, the contour shapes in a LEAP for this case are always circles.

The conditional density in Equation 4 is a probability density function (PDF), but the equation to plot in a LEAP is the probability density element (PDE). For spherical data, the PDE is the PDF without the leading $\sin \theta$ term (Fisher et al. 1987; see also Edwards & Stappers 2004). When $\kappa > 1$, the polarization pattern derived from the PDE is a single set of concentric, circular contours with a peak at the center of the left LEAP hemisphere, where $\theta = 0$ (top panel of Figure 1). When $\kappa < 1$, the conditional density becomes isotropic, and the LEAP will show data points uniformly scattered over both hemispheres. The joint probability density of the orientation angles (Equation 27) is parameterized solely by the polarization signal-to-noise ratio, $s = \mu/\sigma$. The functional form of the joint density is similar to that of the conditional density.

An observational example of this case can be found towards the center of the pulse in PSR B2020+28, as shown in the top panel of Figure 3. The polarization pattern is a set of circularly-shaped contours in a single hemisphere of the LEAP. The cluster of polarization

¹The equivalent of Equation 5 in McKinnon (2003) is used to define κ , instead of κ^2 . The definition used here is preferred because it implies a connection with variance.

data points at this pulse location is clearly a spheroid because its three dimensions are nearly identical (see Figures 3 and 5 of McKinnon 2004).

2.2. Case 2: $\sigma_q = \sigma_u < \sigma_v$

The second case investigates fluctuations in q and u that are equal, $\sigma_q = \sigma_u = \sigma$, but less than those in v by a factor of $(1 + \rho^2)^{1/2}$, where $\rho \geq 0$. This case was evaluated in McKinnon (2006), and considers a system dominated by fluctuations along the polarization vector, as is caused by OPMs. The shape of the q - u - v data point cluster created by these polarization fluctuations is a prolate ellipsoid. Its major axis is parallel to v . The conditional density of the vector's orientation angles is a Bingham-Mardia (BM) bipolar distribution

$$f_2(\theta, \phi | r_o) = \frac{\sin \theta \exp[\kappa^2(\cos \theta + \gamma)^2]}{2\pi w_2(\kappa, \gamma)}. \quad (6)$$

The distribution is parameterized by the constants κ and γ .

$$\kappa^2 = \frac{r_o^2 \rho^2}{2\sigma^2(1 + \rho^2)} \quad (7)$$

$$\gamma = \frac{\mu}{r_o \rho^2} \quad (8)$$

The constant $w_2(\kappa, \gamma)$ normalizes the density and is found by integrating the numerator of Equation 6. The conditional density becomes the Watson bipolar distribution when $\mu = 0$ (McKinnon 2006).

The conditional density can be unimodal or bimodal depending upon the value of γ . When $\gamma > 0$, the PDE always peaks at the center of the left LEAP hemisphere where $\theta = 0$. When $|\gamma| \ll 1$ the polarization pattern is bimodal (i.e. a secondary peak appears at the center of the right LEAP hemisphere where $\theta = \pi$). The patterns are unimodal for larger values of γ . As with Case 1, the shapes of the density's contours are always circles because of the azimuthal symmetry of the problem. The middle panel of Figure 1 shows an example of the PDE from Equation 6.

As shown in McKinnon (2006), the functional form of the joint probability density (Equation 27) is very similar to that of the conditional density. The polarization modulation index, β , determines whether the joint density is bimodal or unimodal. In this case, the modulation index is defined by

$$\beta = \frac{(\sigma_v^2 - \sigma^2)^{1/2}}{\mu} = \frac{\rho}{s}, \quad (9)$$

where $s = \mu/\sigma$ is the ratio of the polarization amplitude to the effective noise of the system. The fluctuations along v that are over and above the effective noise are represented by $\rho\sigma$. When $\beta > 1$, the fluctuations along v exceed the mean polarization, and the joint density is bimodal with data points residing in both LEAP hemispheres. When $\beta < 1$, the mean exceeds the fluctuations, and the joint density is unimodal.

An observational example of this case occurs on the trailing edge of the pulse of PSR B1929+10 (middle panel of Figure 3). There, the polarization pattern consists of a set of circularly-shaped contours in each hemisphere of the LEAP. The contours in the right hemisphere are not centered in the projection because the modes are not precisely orthogonal (McKinnon 2004). The cluster of polarization data points at this location in the pulse has the form of a prolate ellipsoid because two of its dimensions are equal but smaller than the third (Figures 4 and 5 of McKinnon 2004). Another example of this case occurs in the cone emission of PSR B0329+54. Again, the pattern consists of a set of circularly-shaped contours in each hemisphere of the LEAP (Figure 2 of Edwards & Stappers 2004), and the relative dimensions of the data point clusters are consistent with those expected for a prolate ellipsoid (Figure 3 of Edwards & Stappers).

2.3. Case 3: $\sigma_q = \sigma_u > \sigma_v$

To model fluctuations perpendicular to the polarization vector, the fluctuations in q and u are taken to be equal, $\sigma_q = \sigma_u = \sigma(1 + \eta^2)^{1/2}$, but greater than those in v , where $\sigma_v = \sigma$. The constant η denotes the magnitude of the fluctuations perpendicular to the polarization vector, while ρ is reserved to signify the parallel fluctuations. The polarization fluctuations in this case create a q - u - v data point cluster in the shape of an oblate ellipsoid. The minor axis of the ellipsoid is parallel to v . This case does not preclude the possibility of OPMs; it simply stipulates that fluctuations perpendicular to the polarization vector exceed the parallel fluctuations. The conditional density is a BM girdle distribution

$$f_3(\theta, \phi | r_o) = \frac{\sin \theta \exp[-\kappa^2(\cos \theta - \gamma)^2]}{2\pi w_3(\kappa, \gamma)}, \quad (10)$$

where

$$\gamma = \frac{\mu(1 + \eta^2)}{r_o \eta^2} \quad (11)$$

and κ has the same definition as in Case 2, Equation 7, but with ρ replaced by η . The constant $w_3(\kappa, \gamma)$ is a normalization factor. The conditional density is normal in $\cos \theta$ with mean γ and a standard deviation proportional to $1/\kappa$. Since the density is a distribution of $\cos \theta$, which must lie in the range $0 \leq |\cos \theta| \leq 1$, a strict mathematical interpretation

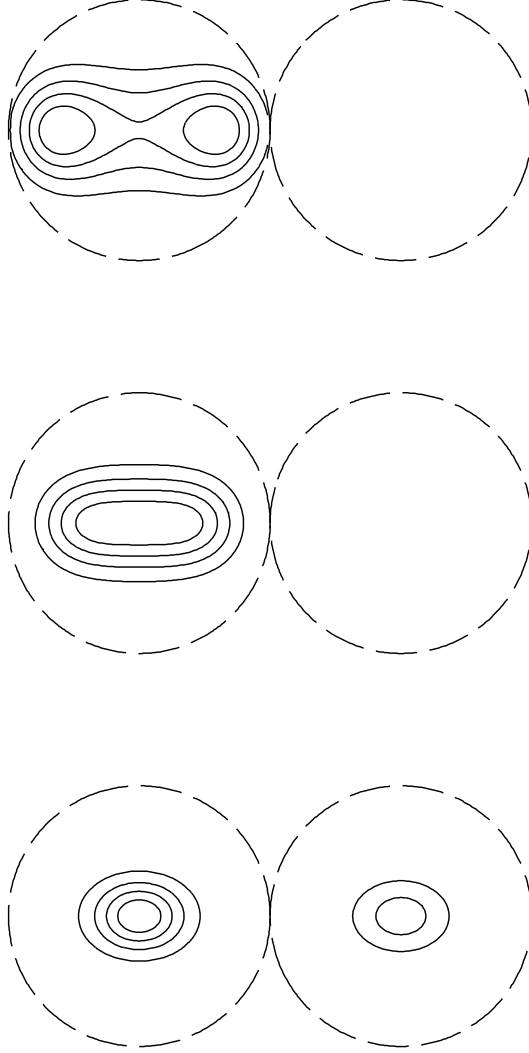


Fig. 2.— Additional examples of possible polarization patterns in pulsar radio emission. *Top panel:* A hybrid of the Bingham-Mardia distribution where the polarization fluctuations are primarily along q (Case 4). This particular pattern was formed with $\kappa = 2$ and $\gamma = 0.65$. *Middle panel:* Same as the top panel but with $\gamma = 1$. *Bottom panel:* Another hybrid of the Bingham-Mardia distribution where the fluctuations in all three dimensions are different, with $\kappa_o = -4$, $\kappa = 3$, and $\gamma = -0.04$ (Case 5). Contour levels are at 0.2, 0.4, 0.6, and 0.8 of the peak value in each projection.

of Equation 10 requires γ to lie in the range $0 \leq |\gamma| \leq 1$. A variant of Equation 10 has been used to model the motion of volcanic hotspots on the surface of the Earth (Bingham & Mardia 1978; Mardia & Gadsden 1977).

As shown in the bottom panel of Figure 1, the polarization pattern formed from the conditional density PDE is an annulus in a single LEAP hemisphere. The PDE peaks at $\cos \theta = \gamma$ for all longitudes, again because of the azimuthal symmetry of the problem. The outer edge of the annulus has a steep slope and its inner edge has a more gradual slope. The sign of γ determines the hemisphere where the annulus resides. When $\gamma = 0$, the PDE peaks at $\theta = \pi/2$, and the pattern contours are concentrated around the equator in each LEAP hemisphere. As γ approaches unity, the annulus collapses into a single cluster with a peak at $\theta = 0$. Unlike the density in Case 2 that can be bimodal, the density in this case is always unimodal.

The shape of the polarization pattern derived from the joint probability density (Equation 27) is again determined by the polarization modulation index, here defined as $\beta = \eta/s$. The polarization pattern is an annulus when the polarization fluctuations are comparable to the mean polarization ($\beta \simeq 1$). The pattern is a single peak at $\theta = 0$ when the polarization fluctuations are less than the mean ($\beta < 1$).

The polarization annulus was first recognized by Melrose et al. (2006) in their attempt to model the polarization pattern observed by Edwards & Stappers (2004) in the core emission of PSR B0329+54. Their numerical model showed that the annulus formed when the polarization amplitude was weak. The analytical model developed here reproduces a similar pattern precisely when μ (i.e. γ) is small or when $\beta \simeq 1$.

2.4. Case 4: $\sigma_q > \sigma_u = \sigma_v$

The fluctuation geometries described in the preceding cases have all been symmetric in azimuth. The symmetry is broken in this case by setting the fluctuations in u and v equal to one another, $\sigma_v = \sigma_u = \sigma$, but less than those in q , $\sigma_q = \sigma(1 + \eta^2)^{1/2}$. Now the shape of the q - u - v data point cluster is a prolate ellipsoid with its major axis oriented along q and thus perpendicular to v . The conditional density is a hybrid of the BM distribution

$$f_4(\theta, \phi | r_o) = \frac{\sin \theta \exp[-\kappa^2(\cos \theta - \gamma)^2] \exp(-\kappa^2 \sin^2 \phi \sin^2 \theta)}{2\pi w_4(\kappa, \gamma)}, \quad (12)$$

where κ and γ have the same definitions as in Case 3, and $w_4(\kappa, \gamma)$ is a constant that normalizes the distribution. Equation 12 is the conditional density of Case 3 (first exponential term in the equation) that is further shaped by a longitude-dependent term (the second

exponential term). The PDE resides in one hemisphere of the LEAP and generally peaks at two locations where $\cos \theta = \gamma$ and $\phi = 0, \pi$. As shown in the top and middle panels of Figure 2, the pattern has a bar shape when $\gamma = 1$, and a bow tie shape when $\gamma < 1$. For even smaller values of γ , the bow tie separates into two distinct peaks.

Again, the polarization modulation index, $\beta = \eta/s$, determines the pattern shape derived from the joint probability density. When $\beta > 1$, the pattern resembles a bow tie. The pattern is a bar when $\beta < 1$.

An observational example of this case appears near the peak of PSR B0823+26 (bottom panel of Figure 3). The polarization pattern consists of a set of highly elongated contours in a single hemisphere of the LEAP. Another observational example of this case may occur in the precursor to the core component of PSR B0329+54, as shown in Figure 2 of Edwards & Stappers (2004). There, an elliptical bar appears superimposed upon a noise background in the left LEAP hemisphere. Only the noise background of uniformly distributed data points appears in the right hemisphere. As shown in their Figure 3, two of the dimensions of the Q-U-V cluster are equal but smaller than the third; therefore, the shape of the cluster is a prolate ellipsoid. For the polarization pattern to be confined primarily to one LEAP hemisphere, the ellipsoid's major axis must be perpendicular to the mode diagonal, as required in this case.

2.5. Case 5: $\sigma_u < \sigma_q = \sigma_v$

The final and most complex, yet general, geometry to consider is when the fluctuations in q and v are greater than those in u, but not necessarily equal to one another. Here, the fluctuations in u are defined as $\sigma_u = \sigma$, and the fluctuations in q and v are $\sigma_q = \sigma(1 + \eta^2)^{1/2}$ and $\sigma_v = \sigma(1 + \rho^2)^{1/2}$, respectively. Generally, the shape of the q-u-v ellipsoid in this case is an irregular ellipsoid that does not have an axis of symmetry. When $\eta = \rho$, the ellipsoid is oblate with its minor axis perpendicular to v, and the conditional density is

$$f_5(\theta, \phi | r_o) = \frac{\sin \theta}{2\pi} \frac{\exp[\kappa^2(\cos \theta + \gamma)^2] \exp(\kappa^2 \sin^2 \phi \sin^2 \theta)}{w_5(\kappa, \gamma)} \quad (13)$$

where κ and γ are now defined by Equations 7 and 8, respectively, under Case 2, and $w_5(\kappa, \gamma)$ is a normalization factor.

When $\eta \neq \rho$, the conditional density is

$$f_5(\theta, \phi | r_o) = \frac{\sin \theta}{2\pi} \frac{\exp[-\kappa_o(\cos \theta - \gamma)^2] \exp(-\kappa^2 \sin^2 \phi \sin^2 \theta)}{w_5(\kappa, \kappa_o, \gamma)} \quad (14)$$

where κ has the same definition as in Cases 3 and 4, and κ_o and γ are given by

$$\kappa_o = \frac{r_o^2(\eta^2 - \rho^2)}{2\sigma^2(1 + \rho^2)(1 + \eta^2)} \quad (15)$$

$$\gamma = \frac{\mu(1 + \eta^2)}{r_o(\eta^2 - \rho^2)} \quad (16)$$

Notice that κ_o and γ can be negative depending upon the values of η and ρ . Equation 14 is very general in that it reproduces the conditional density for Case 4 (Equation 12) when $\rho = 0$. Similarly, it becomes the conditional density for Case 2 (Equation 6) when $\eta = 0$. When $\rho \geq \eta$ such that $|\gamma| < 1$, the polarization pattern derived from Equation 14 is bimodal and very similar to that of Case 2, with the exception that the PDE contours now have elliptical, instead of circular, cross sections because of the asymmetry introduced by the fluctuations in q (see the bottom panel of Figure 2). When $\eta > \rho$, the polarization pattern can be a bar or bow tie in a single hemisphere, as in Case 4, depending upon the value of γ .

An observational example of this case can be found in PSR B0818–13, where the LEAP at the pulse peak is a diffuse structure that resembles a bow tie (Figure 5 of Edwards 2004). The cluster dimensions are not equal to one another, but two of the dimensions are noticeably larger than the third (Edwards, Figure 3), suggesting that the cluster shape is an irregular ellipsoid, as this case requires. To get the bow tie shape in its LEAP, the fluctuations along q would have to be slightly larger than those along v .

3. DEPOLARIZATION BY THE FLUCTUATIONS

The polarization patterns observed in pulsars are indicators of how the orientation angles of a polarization vector fluctuate on the Poincaré sphere. The fluctuations are polarization instabilities that can depolarize the emission. The conditional densities derived in §2 replicate many of the observed polarization patterns, and can be used to quantify the degree of depolarization caused by the fluctuations.

Manchester et al. (1973) first observed that the percentage linear polarization of pulsar radio emission decreased with increasing radio frequency, and Manchester et al. (1975) suggested that the depolarization may arise from an increase in the randomization of polarization position angle. Manchester et al. (1975) and Cordes & Hankins (1977) quantified the stability of the linear polarization with a two-dimensional polarization stability factor,

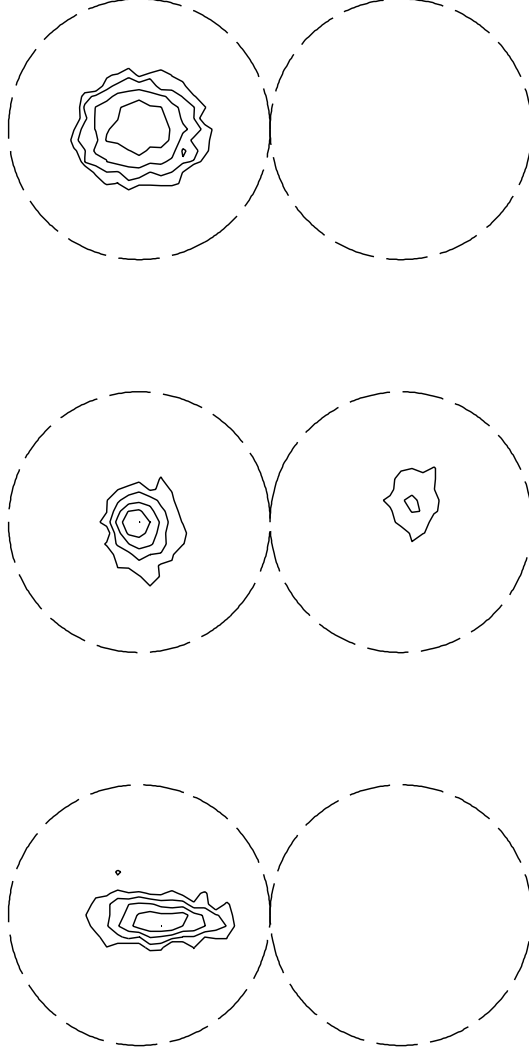


Fig. 3.— Lambert equal area projections of the observed orientation angles of the polarization vector in three pulsars. *Top panel:* Polarization pattern measured towards the center of PSR B2020+28. Contour levels are -12, -9, -6, and -3 decibels (dB) referenced to 0 dB at the peak of the projection. *Middle panel:* Pattern measured on the trailing edge of PSR B1929+10. Contours are -20, -15, -10, and -5 dB. *Bottom panel:* Pattern measured near the peak of PSR B0823+26. Contours are -8, -6, -4, and -2 dB. The data were recorded by Stinebring et al. (1984) with the Arecibo radio telescope at 1404 MHz.

here defined as

$$\sigma_p = \left(\frac{\langle Q \rangle^2 + \langle U \rangle^2}{\langle Q^2 \rangle + \langle U^2 \rangle} \right)^{1/2}. \quad (17)$$

Assuming that the position angle, ψ , is a normal RV with a zero mean and a standard deviation, σ_ψ , Cordes & Hankins (1977) calculated the moments of Q and U to derive a polarization stability factor given by

$$\sigma_p = \exp(-\sigma_\psi^2/2). \quad (18)$$

An identical expression is used to describe the depolarization caused by stochastic Faraday rotation in the interstellar medium (e.g. Spangler 1982; Melrose & Macquart 1998).

Using the same methodology described in §2, McKinnon (2003) showed that the conditional density of the position angle follows a von Mises distribution

$$f(\psi|r_o) = \frac{\exp(\kappa^2 \cos 2\psi)}{\pi I_0(\kappa^2)}, \quad (19)$$

where $I_0(x)$ is the modified Bessel function of order zero and κ is inversely related to the position angle dispersion. The polarization stability factor derived from the von Mises distribution is

$$\sigma_p = \frac{I_1(\kappa^2)}{I_0(\kappa^2)}, \quad (20)$$

where $I_1(x)$ is the modified Bessel function of first order. When the fluctuations in ψ are small ($\kappa \gg 1$), the von Mises distribution is almost indistinguishable from a normal distribution with a standard deviation of $\sigma_\psi = (2\kappa)^{-1}$. Of the two distributions, the von Mises distribution is the more accurate representation of position angle fluctuations because ψ is distributed on a semi-circle, not a line, and lies in the range $0 \leq \psi < \pi$, instead of $-\infty \leq \psi < \infty$ (Fisher et al. 1987). The stability factors derived from the two distributions are compared in the top left panel of Figure 4.

The observations of Edwards (2004) and Edwards & Stappers (2004), however, have clearly shown that the fluctuations occur in all three Stokes parameters, and not just in Q and U. Consequently, polarization fluctuations in the three dimensional case cause the vector colatitude to vary in addition to its longitude (position angle). The depolarization can be quantified by extending the definition of the polarization stability factor to

$$\sigma_p = \left(\frac{\langle Q \rangle^2 + \langle U \rangle^2 + \langle V \rangle^2}{\langle Q^2 \rangle + \langle U^2 \rangle + \langle V^2 \rangle} \right)^{1/2}. \quad (21)$$

For any joint probability density of θ and ϕ that is properly normalized, the sum of the second moments of the Stokes parameters is constant because of the definitions of the Stokes

parameters and trigonometric identities. The first moments of Q and U are equal to zero for all the distributions derived in §2. Therefore, the only term that contributes to the stability factor is the first moment of V.

The polarization stability factor derived from the Fisher distribution (Case 1) is

$$\sigma_p = \coth(\kappa^2) - \frac{1}{\kappa^2}, \quad (22)$$

and is shown in the top right panel of Figure 4. Very little depolarization occurs when the fluctuations are small ($\kappa \gg 1$), but the depolarization can be significant when the fluctuations are large ($\kappa \simeq 1$).

The polarization stability factor derived from the BM bipolar distribution (Case 2) is

$$\sigma_p = \frac{\exp[\kappa^2(1 + \gamma^2)] \sinh(2\kappa^2\gamma)}{\kappa^2 w_2(\kappa, \gamma)} - \gamma, \quad (23)$$

where the constant $w_2(\kappa, \gamma)$ is given by

$$w_2(\kappa, \gamma) = \int_{\gamma-1}^{\gamma+1} \exp(\kappa^2 x^2) dx. \quad (24)$$

The stability factor for Case 2 is plotted against κ for different values of γ in the bottom left panel of Figure 4. The fluctuations can depolarize the radiation, but the figure shows that the depolarization is more pronounced for small values of γ .

The polarization stability factor derived from the BM girdle distribution (Case 3) is

$$\sigma_p = \gamma - \frac{\exp[-\kappa^2(1 + \gamma^2)] \sinh(2\kappa^2\gamma)}{\kappa^2 w_3(\kappa, \gamma)}. \quad (25)$$

The constant $w_3(\kappa, \gamma)$ is

$$w_3(\kappa, \gamma) = \frac{\sqrt{\pi}}{2\kappa} \{\text{erf}[\kappa(1 - \gamma)] + \text{erf}[\kappa(1 + \gamma)]\}. \quad (26)$$

The stability factor for Case 3 is shown in the bottom right panel of Figure 4. As with Case 2, the depolarization is more severe for small values of γ . The stability factor approaches $\sigma_p = \gamma$ when $\kappa \gg 1$.

The effect of κ and γ on the frequency-dependent polarization can be summarized as follows. The term κ represents the magnitude of the fluctuations and sets the overall size of the polarization pattern; larger patterns are formed from smaller values of κ . The frequency dependence of κ may be set by the process responsible for the polarization fluctuations. The

term γ is proportional to μ , and thus is set by the OPMs or a process intrinsic to the emission mechanism. Its frequency dependence may be determined by the spectral index of the individual modes (e.g. Karastergiou et al. 2005; Smits et al. 2006; Johnston et al. 2008) or that of the emission’s intrinsic polarization. As can be seen from Figure 4, the depolarization caused by pure fluctuations alone (the Fisher distribution from Case 1, top right panel) forms a rough, upper envelope to the depolarization caused by the other fluctuation geometries. The depolarization becomes more substantial in Cases 2 and 3 (bottom panels of the Figure) as the value of γ decreases. In other words, the depolarization is influenced more by the intrinsic effects represented by γ than by the polarization fluctuations represented by κ . Therefore, the main conclusion to draw from this polarization stability analysis is pulsar-intrinsic effects are more effective at depolarizing the emission than random fluctuations in the orientation of the polarization vector.

4. POSSIBLE ORIGIN OF PERPENDICULAR FLUCTUATIONS

A single, physical process is not likely to be responsible for all the polarization patterns we observe. As mentioned in the Introduction, the origin of the simple polarization patterns is qualitatively understood, particularly in the case of OPMs where the patterns are formed by fluctuations parallel to the mode polarization vectors. The origin of the more complicated patterns created by perpendicular polarization fluctuations is not understood. But as discussed below, they may arise from a stochastic version of GFR or scattering in the pulsar magnetosphere.

4.1. Stochastic Version of Generalized Faraday Rotation

In general terms, Faraday rotation is the physical process that alters the difference between the phases of the modes as they propagate through a plasma (Melrose 1979), regardless of the particle energy in the plasma, the strength of the magnetic field threading the plasma, or the coherence of the modes. The modes are incoherent when the difference in their phases at a given wavelength is large ($\Delta\chi \gg 1$) and are coherent (coupled) as long as the phase difference is small ($\Delta\chi < 1$). The modes retain their individual polarization identity in an observation when they are incoherent, but effectively lose their identity when they are coherent. Faraday rotation can become stochastic when the fluctuations in phase difference are large ($\sigma_\chi \gg 1$), in which case $\Delta\chi$ can be treated as a random variable (Lee & Jokipii 1975; Simonetti et al. 1984; Melrose & Macquart 1998).

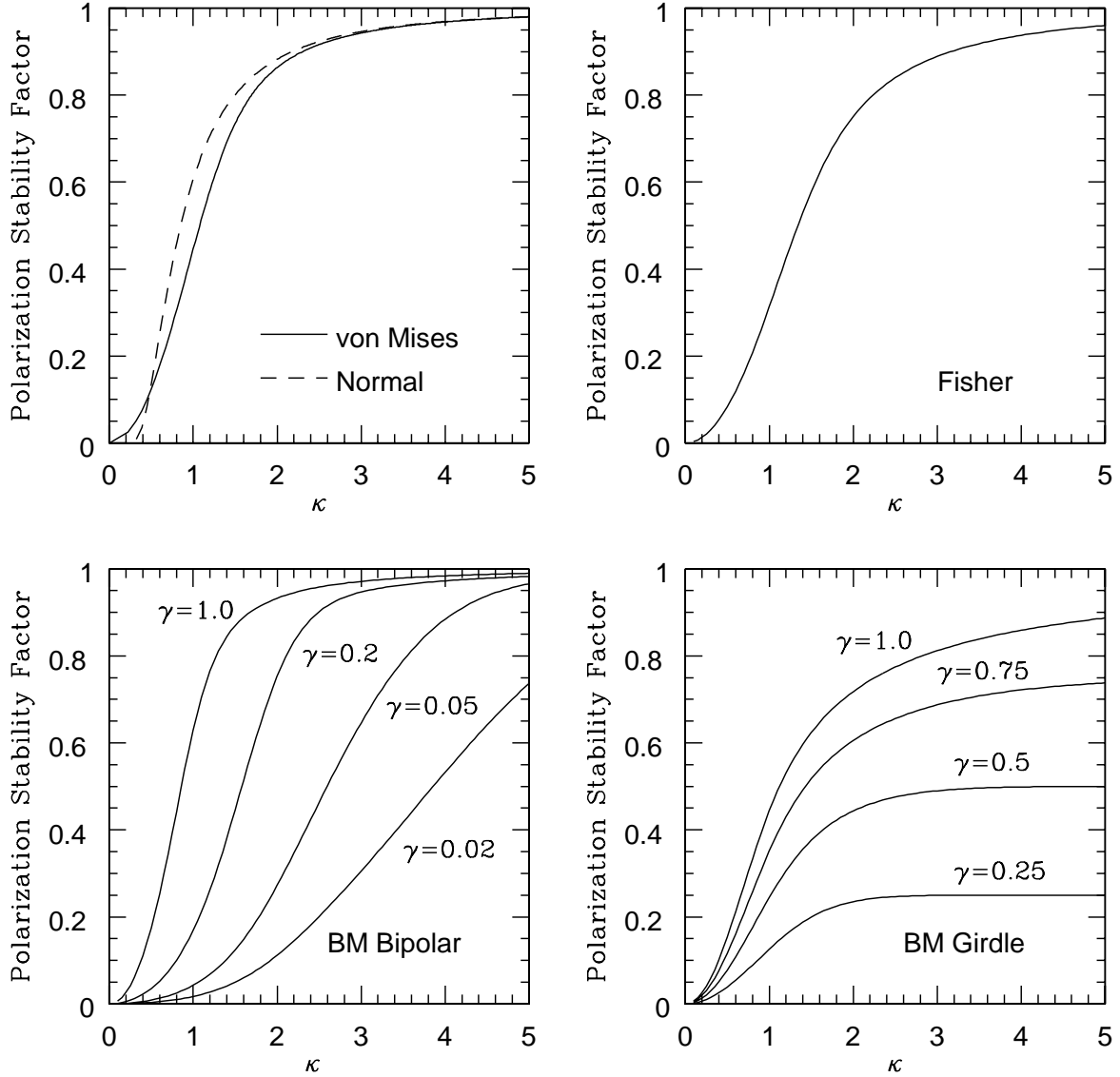


Fig. 4.— The dependence of the polarization stability factor upon different types of fluctuations in the position angle or colatitude of the polarization vector. The top left panel shows the stability factor when the fluctuations in position angle follow the two-dimensional von Mises and normal distributions. The top right panel shows the stability factor when the colatitude of the polarization vector fluctuates according to the three-dimensional Fisher distribution (Case 1). The stability factors determined from the Bingham-Mardia bipolar distribution (Case 2) and the Bingham-Mardia girdle distribution (Case 3) are shown in the bottom left and right panels, respectively, for different values of γ . The factors are plotted versus κ , which is related inversely to the dispersion in colatitude or position angle.

GFR alters the component of the radiation’s polarization vector that is perpendicular to the polarization vectors of the plasma’s wave propagation modes. For any plasma, the unit vectors representing the polarization states of the two modes are anti-parallel on a diagonal through the Poincaré sphere. For the cold, weakly-magnetized plasma that is the interstellar medium (ISM), the propagation modes are circularly polarized, and the mode diagonal defined by their polarization vectors connects the poles of the Poincaré sphere. Faraday rotation in the ISM causes the orientation of the radiation’s polarization to vary in a plane perpendicular to the mode diagonal, either on the Poincaré sphere’s equator or on a small circle parallel to it, depending upon the polarization state of the plasma-incident radiation. For the relativistic plasma in the strong magnetic field of a pulsar’s magnetosphere, the modes are thought to be linearly polarized (Melrose 1979; Allen & Melrose 1982; Barnard & Arons 1986) so that the mode diagonal lies in the equator of the Poincaré sphere. The modes in a relativistic, magnetized plasma of a synchrotron radio source or pulsar wind are, in general, elliptically polarized (Kennett & Melrose 1998; Pacholczyk & Swihart 1970; Sincell & Krolik 1992). In these latter cases, GFR causes the polarization vector to rotate on a small circle in the Poincaré sphere that is perpendicular to and centered on the mode diagonal (e.g. Figure 3 of Kennett & Melrose 1998). If the modes are coherent, GFR causes the amplitude of the linear and circular polarization to vary periodically (Pacholczyk & Swihart 1970; Cocke & Pacholczyk 1976).

For GFR to occur, the polarization of the radiation incident on the plasma must be different from the polarization of the plasma’s wave propagation modes (e.g. Pacholczyk & Swihart 1970). How this might occur in a pulsar’s magnetosphere can be understood if we view the magnetosphere as being composed of layers, where the properties of the wave propagation modes are constant within a given layer, but different between layers. The mode properties, such as their indices of refraction and polarization states, are likely to vary quickly with distance, r , from the center of the pulsar, because both the particle density and magnetic field strength are thought to decrease as r^{-3} (Goldreich & Julian 1969). For simplicity, let us assume the radiation is generated in the lowest magnetospheric layer and its polarization state is identical to that of the wave modes in the layer to ensure efficient coupling between the generation and propagation of the radiation. The radiation’s polarization is unaffected in the lowest layer, but gets slightly altered by GFR in subsequent layers, because the polarization of the radiation incident on each layer is different from the polarization of that layer’s propagation modes. The radiation’s polarization in each layer then contains a component that is perpendicular to the mode polarization because of GFR. Ultimately, a polarization limiting region (PLR) is reached in the upper layers of the magnetosphere where GFR is no longer effective in altering the radiation’s polarization (Melrose 1979; Kennett & Melrose 1998). The PLR occurs where, or when, $\Delta\chi = 1$. At

or just beyond the PLR, the radiation must couple to the ISM wave modes for propagation through the ISM (Stinebring 1982). With this simple cartoon, we see how GFR may be capable of producing a polarization component that is perpendicular to the polarization of the wave propagation modes.

The relatively long wavelength ($\lambda > 10$ cm) observations of individual pulse polarization conducted to date suggest that the wave propagation modes in pulsar radio emission are incoherent (MS1; MS2). Consequently, the differences in mode phases must be large, implying GFR is operative in the pulsar magnetosphere. Furthermore, the emission’s intensity and polarization are highly variable, most likely due to rapid changes, both spatially and temporally, in the flowrate and physical properties of the magnetospheric plasma. This in turn suggests that the fluctuations in the mode phase difference, σ_ψ , are also very large. We are then led to the prospect that GFR in the pulsar magnetosphere is likely to be stochastic. This interpretation is consistent with the analysis in §2 where the orientation angles of the polarization vectors are treated as random variables.

The theory of stochastic Faraday rotation in the ISM is well-developed (e.g. Spangler 1982; Simonetti et al. 1984; Melrose & Macquart 1998). The theory probes a two dimensional problem, in the Stokes parameters Q and U, where the fluctuations in the position angle of the linear polarization vector map directly to the fluctuations in the mode phase difference. The extension of the theory to the more general, three dimensional case (Q, U, and V) of stochastic GFR has not been made and is beyond the scope of this paper. In the absence of the theory, knowing that the conditional densities derived in §2 are reasonable approximations to the polarization patterns we observe, and realizing that stochastic GFR may occur in the magnetosphere, we are faced with the possibility that some subset of these conditional densities, or some other joint probability density, may describe how GFR causes the orientation of a pulsar’s polarization vector to fluctuate. Interestingly, the polarization stability analysis in §3 produces the same conclusions developed by Melrose & Macquart (1998) in their assessment of depolarization by stochastic Faraday rotation in the ISM. Specifically, when the conditional densities are used to calculate the moments of the Stokes parameters, the first moments decay and the sum of their second moments remains constant. In fact, the radiative transfer equation for the Stokes parameters (e.g. Equation 1 of Kennett & Melrose 1998) requires the second moment of the polarization, $p^2 = q^2 + u^2 + v^2$, to remain constant as the radiation propagates through the plasma. All of the conditional and joint probability densities listed in §2 and the Appendix comply with this requirement.

4.2. Scattering in the Magnetosphere

Edwards & Stappers (2004) simulated the polarization patterns in the core component of PSR B0329+54. They suggested that the modes are not precisely orthogonal, and retained the assumption of superposed modes. More importantly, and in contrast to the models discussed in §2, they also proposed that the orientation angles for the polarization vector of one mode are highly dispersed while the angles of the other mode are not. They attributed the orientation angle fluctuations to GFR. More specifically, however, their model is consistent with any mechanism that selectively alters the orientation angles of only one mode. Melrose et al. (2006) also modeled the polarization patterns in the core component of PSR B0329+54 using assumptions similar to those of Edwards & Stappers. They invoked the non-orthogonality of the modes and required the fluctuations in the orientation angles of one mode to be different from those in the other. But unlike Edwards & Stappers, they suggested that the modes are disjoint (i.e. they occur separately, not simultaneously) part of the time, and did not specifically advocate a physical mechanism for the cause of the orientation angle fluctuations.

One mechanism that may alter the orientation angles of one polarization mode and not the other is scattering in the pulsar magnetosphere (Blandford & Scharlemann 1976; Sincell & Krolik 1992; Lyubarskii & Petrova 1996; Petrova 2008). Induced scattering may occur in the magnetosphere because large photon occupation numbers are implied by the high brightness temperatures observed in the radio emission. When the radiation frequency, ω , is much less than the electron gyrofrequency, ω_B , as might be expected near the stellar surface, the only wave propagation mode that has a non-zero scattering cross section is the ordinary mode (O-mode), which is polarized in the plane defined by the wave vector, \mathbf{k} , and the ambient magnetic field, \mathbf{B} (Blandford & Scharlemann 1976; Sincell & Krolik 1992). This occurs for two reasons. First, the extreme strength of the field ($B \simeq 10^{12}$ G) causes the electrons in the plasma to occupy their lowest Landau level, such that their motion is constrained along the field, like a bead on a wire. Second, in an overly simplistic description, only an incident O-mode wave can accelerate an electron along the field, thus causing it to radiate, because it is the only mode having a component to its electric field that is parallel to the ambient magnetic field. The extra-ordinary mode (X-mode) cannot accelerate an electron along the field because its electric field is always perpendicular to the magnetic field. The scattering cross section varies as $\sin^2 \theta$ (Blandford & Scharlemann 1976), where θ is now the angle between \mathbf{k} and \mathbf{B} , and no scattering will occur if \mathbf{k} and \mathbf{B} are parallel ($\theta = 0$). The observed polarization of the scattered radiation depends upon the geometry of the magnetic field in the scattering region, as projected on the plane of the sky, and the temporally and spatially varying distribution of charged particles along the magnetic field lines.

Petrova (2008) has suggested that induced scattering at different altitudes within the magnetosphere may lead to a depolarization of the radiation. The scattered radiation from different altitudes may have different position angles, and it is the superposition of these waves with different position angles that leads to the depolarization. This scenario is qualitatively consistent with what is described in §2, Cases 3 and 4.

In summary, the empirical models appear to place three requirements on the physical processes that create the more complex polarization patterns we observe. First, the polarization must have a large modulation index, through a combination of large polarization fluctuations and a small mean polarization. Second, the processes must create fluctuations in polarization that are both parallel and perpendicular to the mean polarization vector. Third, in some cases, the process may create fluctuations in the orientation of the polarization vector of one orthogonal mode that exceed those in the other mode.

5. DISCUSSION

A fundamental question remains for the observation of PSR B0329+54 by Edwards & Stappers (2004). Why does the polarization annulus appear in the core component of the pulsar but not in its conal outriders? The annulus must be intrinsic to the pulsar because a propagation effect in the pulsar wind or the ISM presumably would affect the core and cone emission in a similar fashion. Explanations for the difference may reside in the distinction between core and cone emission made by Rankin (1983; 1990). Cone emission has a moderate spectral index and can be highly linearly polarized. It is thought to originate high above the pulsar polar cap. Core emission, on the other hand, has a steep spectral index, and its polarization signature is often a change in the handedness of the circular polarization near the core peak. It is thought to originate at or near the polar cap. The core and cone radiation from PSR B0329+54 appear to follow this general characterization of the emission components (Karastergiou et al. 2001). We can surmise that GFR occurs throughout the pulse of PSR B0329+54 because observations (Edwards & Stappers 2004) indicate that independent OPMs occur at most locations within its pulse. Of course, the core emission would be more susceptible to GFR because its propagation path length is presumably much larger than that for the cone emission. Stochastic GFR may occur predominantly near the stellar surface where a turbulent plasma outflow causes fluctuations in the mode phase difference. Stochastic GFR may get suppressed in the propagation region for the cone emission because the cross section of the plasma flux tube increases with distance from the star and, thus, the plasma outflow becomes more laminar. Alternatively, a popular model for pulsar radio emission (e.g. Ruderman & Sutherland 1975) calls for an intense photon beam to be created

by primary charged particles that are accelerated in a voltage potential gap near the stellar surface. These photons produce secondary pairs of charged particles that go on to radiate via coherent curvature radiation, for example. In this scenario, perhaps the polarization annulus appears only in the core emission because only the photon beam can provide the large photon occupation numbers that are conducive to induced scattering. Scattering would be most evident where the wave vector of the O-mode radiation is perpendicular to the ambient magnetic field, as might be expected in the multi-polar structure of the field near the stellar surface where the core emission is thought to originate. Furthermore, the specific scattering process described in §4 will not occur higher in the magnetosphere where the electrons can occupy higher Landau levels and the cyclotron frequency can approach the radiation frequency. Finally, the presence of both the polarization annulus and the sign-changing circular polarization in the core component of PSR B0329+54 begs a secondary question of whether the two phenomena are related or entirely coincidental. Single pulse observations of other pulsars dominated by core emission, such as PSR B1933+16, could test whether the phenomena are associated with one another.

The analytical model of pulsar polarization presented in this paper can describe most, but not all, of the polarization patterns observed in PSR B0329+54. In the cone emission of the pulsar, the LEAPs show a data cluster with circular cross-section in each hemisphere, consistent with the pattern described in Case 2. The cluster in the precursor to the core component has the shape of an elliptical bar, which is the pattern produced by Case 4. The LEAP observed at the core component shows an elliptical bar in one hemisphere and a partial annulus in the other. None of the cases considered in §2 can reproduce this pattern. Additional assumptions, such as those described by Melrose et al. (2006) and Edwards & Stappers (2004), must be invoked to model the polarization at this pulse location.

The oft-stated objective of polarization observations of individual pulses (e.g. Manchester et al. 1975; Stinebring et al. 1984) is to understand the radio emission mechanism of pulsars. Progress has been made on this front, particularly with total intensity measurements that reveal a carousel of subbeams circulating about the star’s magnetic pole (e.g. Deshpande & Rankin 1999). But in most cases, propagation effects in the pulsar magnetosphere, not radio emission mechanisms, are invoked to interpret the results of these observations. Afterall, a multitude of propagation effects in the ISM complicates our reception of the pulsar signal, so we should not be surprised that propagation effects in the pulsar magnetosphere complicate our view of what happens there. For example, the occurrence of OPMs has been attributed to the birefringence of the magnetospheric plasma above the pulsar polar cap (Allen & Melrose 1982; Barnard & Arons 1986; Petrova 2001). Cyclotron absorption high in the magnetosphere (Luo & Melrose 2001; Melrose 2003) has been proposed as a possible origin of circular polarization in the emission. In this paper, GFR and scattering are sug-

gested as possible candidates for the origin of some polarization patterns. Individually and collectively, these propagation effects can obscure the polarization of the underlying emission mechanism. If these interpretations are correct, they imply that single pulse polarization observations are best suited for probing propagation effects in pulsar magnetospheres. The emission mechanism may reveal its secrets through total intensity observations, similar to the high time resolution measurements by Hankins & Eilek (2007) who recently found multiple, narrow, radiation bands in the emission from the Crab pulsar.

6. CONCLUSIONS

An empirical, analytical model of pulsar polarization has been generalized to accommodate a wide variety of polarization fluctuation geometries. The model is based upon the proposition that the observed polarization of pulsar radio emission is due to the incoherent superposition of highly polarized orthogonal modes. For the modes to propagate independently, generalized Faraday rotation may be operative in the pulsar magnetosphere for the modes to get significantly out of phase. The model replicates the polarization patterns observed in many objects and reproduces the numerical results from other work. When the fluctuations are parallel to the polarization vectors of the wave propagation modes, the patterns consist of two tight clusters, each in a separate hemisphere of the Poincaré sphere. The patterns assume shapes of bars, bow ties, and annuli when the fluctuations are perpendicular to the vectors. The more interesting patterns occur when the polarization modulation index exceeds unity. The diverse polarization patterns are not likely to originate from the same physical process. The parallel polarization fluctuations are caused by fluctuations in the polarized intensities of the orthogonal modes. The perpendicular fluctuations may be caused by a stochastic version of generalized Faraday rotation, which would require large fluctuations in the difference between mode phases. An expansion of the two dimensional theory of stochastic Faraday rotation in the ISM to the three dimensional case for pulsar magnetospheres may aid the interpretation of the observed polarization patterns. An alternative model suggests that one mode may experience fluctuations perpendicular to its polarization vector while the other does not, implying the presence of a mode-selective, random process, such as scattering in the pulsar magnetosphere. The polarization patterns reflect polarization instabilities that can depolarize the emission in a way that is similar to stochastic Faraday rotation in the ISM. The depolarization has been quantified with a polarization stability factor for the simpler fluctuation geometries. The stability factors imply that pulsar-intrinsic effects are more effective in depolarizing the emission than fluctuations in the orientation of its polarization vector. For all geometries evaluated with the model, the joint probability density of the polarization vector’s orientation angles follows the same

functional form apart from parameters determined by the geometry of the polarization fluctuations. The conditional density of the orientation angles in all cases follows the Fisher and Bingham-Mardia family of distributions.

I thank Dan Stinebring for providing the data used in the analysis.

APPENDIX

Joint Probability Density of Colatitude and Longitude

The basic functional form of the joint probability density of a polarization vector's colatitude, θ , and longitude, ϕ , for all cases considered in §2 is given by

$$g(\theta, \phi) = zC \frac{\sin \theta}{4\pi} \left\{ \exp\left(\frac{y^2}{2}\right) \left[1 + \operatorname{erf}\left(\frac{y}{\sqrt{2}}\right) \right] (1 + y^2) + y \sqrt{\frac{2}{\pi}} \right\}, \quad (27)$$

where $\operatorname{erf}(x)$ is the error function, C is a constant, and the parameters y and z are functions of θ and ϕ determined by the geometry of the polarization fluctuations. The analytical expressions for C , y , and z for each case are listed below.

Case 1:

$$C = \exp\left(-\frac{s^2}{2}\right) \quad (28)$$

$$y(\theta, \phi) = s \cos \theta \quad (29)$$

$$z(\theta, \phi) = 1 \quad (30)$$

Case 2:

$$C = \exp\left[-\frac{s^2}{2(1 + \rho^2)}\right] \quad (31)$$

$$y(\theta, \phi) = \frac{s \cos \theta}{[(1 + \rho^2 \sin^2 \theta)(1 + \rho^2)]^{1/2}} \quad (32)$$

$$z(\theta, \phi) = \frac{(1 + \rho^2)}{(1 + \rho^2 \sin^2 \theta)^{3/2}} \quad (33)$$

Case 3:

$$C = \exp\left(-\frac{s^2}{2}\right) \quad (34)$$

$$y(\theta, \phi) = s \cos \theta \left(\frac{1 + \eta^2}{1 + \eta^2 \cos^2 \theta} \right)^{1/2} \quad (35)$$

$$z(\theta, \phi) = \frac{(1 + \eta^2)^{1/2}}{(1 + \eta^2 \cos^2 \theta)^{3/2}} \quad (36)$$

Case 4:

$$C = \exp \left(\frac{-s^2}{2} \right) \quad (37)$$

$$y(\theta, \phi) = s \cos \theta \left[\frac{1 + \eta^2}{1 + \eta^2 (\cos^2 \theta + \sin^2 \theta \sin^2 \phi)} \right]^{1/2} \quad (38)$$

$$z(\theta, \phi) = \frac{(1 + \eta^2)}{[1 + \eta^2 (\cos^2 \theta + \sin^2 \theta \sin^2 \phi)]^{3/2}} \quad (39)$$

Case 5:

$$C = \exp \left[\frac{-s^2}{2(1 + \rho^2)} \right] \quad (40)$$

$$y(\theta, \phi) = s \cos \theta \left(\frac{1 + \eta^2}{1 + \rho^2} \right)^{1/2} \left\{ \frac{1}{(1 + \eta^2) + \sin^2 \theta [(\rho^2 - \eta^2) + \eta^2(1 + \rho^2) \sin^2 \phi]} \right\}^{1/2} \quad (41)$$

$$z(\theta, \phi) = \frac{(1 + \eta^2)(1 + \rho^2)}{\{(1 + \eta^2) + \sin^2 \theta [(\rho^2 - \eta^2) + \eta^2(1 + \rho^2) \sin^2 \phi]\}^{3/2}} \quad (42)$$

Case 5 provides a general joint probability density for θ and ϕ . It becomes the joint density for Case 1 when $\eta = \rho = 0$, for Case 2 when $\eta = 0$, and for Case 4 when $\rho = 0$. When $s = 0$, the joint probability density becomes $g(\theta, \phi) = z(\theta, \phi) \sin \theta / 4\pi$ for all cases since both C and the bracketed term in Equation 27 become equal to one.

REFERENCES

- Allen, M. C. & Melrose, D. B. 1982, *Proc. Astron. Soc. Aust.*, 4, 365
- Barnard, J. J. & Arons, J. 1986, *ApJ*, 302, 138
- Bingham, C. & Mardia, K. V. 1978, *Biometrika*, 65, 379
- Blandford, R. D. & Scharlemann, E. T. 1976, *MNRAS*, 174, 59
- Chandrasekhar, S. 1960, *Radiative Transfer*, (New York: Dover)
- Cocke, W. J. & Pacholczyk, A. G. 1976, *ApJ*, 204, L13
- Cordes, J. M. & Hankins, T. H. 1977, *ApJ*, 218, 484
- Deshpande, A. A. & Rankin, J. M. 1999, *ApJ*, 524, 1008
- Edwards, R. T. 2004, *A&A*, 426, 677
- Edwards, R. T. & Stappers, B. W. 2004, *A&A*, 421, 681
- Fisher, N. I, Lewis, T., & Embleton, B. J. J. 1987, *Statistical Analysis of Spherical Data*, (Cambridge: Cambridge)
- Goldreich, P. & Julian, 1969, *ApJ*, 157, 869
- Hankins, T. H. & Eilek, J. A. 2007, *ApJ*, 670, 693
- Ishimaru, A. 1978, *Wave Propagation and Scattering in Random Media*, (New York: Academic)
- Johnston, S., Karastergiou, A., Mitra, D., & Gupta, Y. 2008, *MNRAS*, 388, 261
- Karastergiou, A., von Hoensbroech, A., Kramer, M., Lorimer, D. R., Lyne, A. G., Doroshenko, O., Jessner, A., Jordan, C., & Wielebinski, R. 2001, *A&A*, 379, 270
- Karastergiou, A., Johnston, S., & Kramer, M. 2003, *A&A*, 404, 325
- Karastergiou, A., Johnston, S., & Manchester, R. N. 2005, *MNRAS*, 359, 481
- Kennett, M. & Melrose, D. 1998, *PASA*, 15, 211
- Lee, L. C. & Jokipii, J. R. 1975, *ApJ*, 196, 695
- Luo, Q. & Melrose, D. B. 2001, *MNRAS*, 325, 187
- Lyubarskii, Y. E. & Petrova, S. A. 1996, *Astron. Let.*, 22, 399
- Manchester, R. N., Taylor, J. H., & Huguenin, G.R. 1973, *ApJ*, 179, L7
- Manchester, R. N., Taylor, J. H., & Huguenin, G. R. 1975, *ApJ*, 196, 83
- Mardia, K.V. & Gadsden, R. J. 1977, *Applied Statistics*, 26, 238
- Melrose, D. B. 1979, *Aust. J. Phys.*, 32, 61

- Melrose, D. B. 2003, in ASP Conf. Ser. 302, Radio Pulsars, ed. M. Bailes, D. J. Nice & S. Thorsett (San Francisco: ASP), 179
- Melrose, D. B. & Macquart, J.-P. 1998, ApJ, 505, 921
- Melrose, D., Miller, A., Karastergiou, A., Luo, Q. 2006, MNRAS, 365, 638
- McKinnon, M. M. 2003, ApJS, 148, 519
- McKinnon, M. M. 2004, ApJ, 606, 1154
- McKinnon, M. M. 2006, ApJ, 645, 551
- McKinnon, M. M. & Stinebring, D. R. 1998, ApJ, 502, 883
- McKinnon, M. M. & Stinebring, D. R. 2000, ApJ, 529, 435
- Pacholczyk, A. G. & Swihart, T. L. 1970, ApJ, 161, 415
- Petrova, S. A. 2001, A&A, 378, 883
- Petrova, S. A. 2008, MNRAS, 385, 2143
- Rankin, J. M. 1983, ApJ, 274, 333
- Rankin, J. M. 1990, ApJ, 352, 247
- Ruderman, M. A. & Sutherland, P. G. 1975, ApJ, 196, 51
- Simonetti, J. H., Cordes, J. M., & Spangler, S. R. 1984, ApJ, 284, 126
- Sincell, M. W. & Krolik, J. H. 1992, ApJ, 395, 553
- Smits, J. M., Stappers, B. W., Edwards, R. T., Kuipers, J., and Ramachandran, R. 2006, A&A, 448, 1139.
- Spangler, S. R. 1982, ApJ, 261, 310
- Stinebring, D. R. 1982, PhD dissertation, Cornell University
- Stinebring, D. R., Cordes, J. M., Rankin, J. M., Weisberg, J. M., & Boriakoff, V. 1984, ApJS, 55, 247
- von Hoensbroech, A., Kijak, J., & Krawczyk, A. 1998, A&A, 334, 571

Table 1. Summary of Fluctuation Geometry Cases

Case	Fluctuations	Cluster Shape	Axis Orientation	Conditional Density
1	$\sigma_q = \sigma_u = \sigma_v$	Spheroid	NA	Fisher
2	$\sigma_q = \sigma_u < \sigma_v$	Prolate Ellipsoid	Parallel	BM bipolar
3	$\sigma_q = \sigma_u > \sigma_v$	Oblate Ellipsoid	Parallel	BM girdle
4	$\sigma_q > \sigma_u = \sigma_v$	Prolate Ellipsoid	Perpendicular	BM hybrid
5	$\sigma_u < \sigma_q, \sigma_v$	Irregular Ellipsoid	σ -dependent	BM hybrid